

# Constraining Inflation Models with Spinning Voids

Geonwoo Kang and Joung hun Lee

*Astronomy Program, Department of Physics and Astronomy, Seoul National University,  
Seoul 08826, Republic of Korea*

## ABSTRACT

We present a powerful new diagnostics by which the running of scalar spectral index of primordial density fluctuations can be tightly and independently constrained. This new diagnostics utilizes coherent rotation of void galaxies, which can be observed as redshift asymmetry in opposite sides dichotomized by the projected spin axes of hosting voids. Comparing the numerical results from the AbacusSummit of cosmological simulations, we derive a non-parametric model for the redshift asymmetry distribution of void galaxies, which turns out to be almost universally valid for a very broad range of cosmologies including dynamic dark energy models with time-dependent equation of states as well as the  $\Lambda$ CDM models with various initial conditions. We discover that the universality of this model breaks down only if the running of scalar spectral index deviates from zero, detecting a consistent trend that a more positive (negative) running yields a lower (higher) redshift asymmetry of voids than the model predictions. Given that non-standard inflations usually predict non-zero runnings of the spectral index and that the redshift asymmetry distribution of voids is a readily observable quantity, we conclude that this new diagnostics will pave another path toward understanding the true mechanism of inflation.

*Subject headings:* Unified Astronomy Thesaurus concepts: Cosmology (343); Large-scale structure of the universe (902)

## 1. Introduction

The cosmic web is a jargon coined to describe a strikingly anisotropic interconnectivity that the galaxies exhibit in their spatial distributions when viewed on the largest-scale (Bond et al. 1996). It has four distinct segments: knots, filaments, sheets and voids, categorized by the dimensions of their geometrical shapes and characterized by their unique properties (Hahn et al. 2007). The first structures ever formed via gravitational collapse of density

inhomogeneities are the one-dimensional (1D) sheets, sometimes called the Zel'dovich pancakes (Zel'dovich 1970; Kuhlman et al. 1996). Meanwhile, the most anisotropic structures hosting the largest galaxy population are the two-dimensional (2D) filaments (Ganeshaiah Veena et al. 2019). At the junctions of multiple filaments are located the zero-dimensional (0D) knots where the largest bound objects, galaxy clusters, reside. These three over-dense segments have been the focus of extensive studies to understand the origin and evolution of the cosmic web and to find its connection to the initial conditions of the universe (e.g., Pearson & Coles 1995; Bond et al. 1996; Shandarin et al. 2004; Sousbie et al. 2008; Park & Lee 2009; Cautun et al. 2014; Wang et al. 2021; Wilding et al. 2021; Feldbrugge et al. 2023; Feldbrugge & van de Weygaert 2023; Galárraga-Espinosa et al. 2024; Lu et al. 2024; Feldbrugge & van de Weygaert 2025, and references therein).

Recently, growing cosmological interest has been directed toward the fourth type of the cosmic web, *the voids*, markedly 3D structures wrapped by filaments and sheets, occupying the largest volumes of the universe, but almost devoid of galaxies (Zeldovich et al. 1982; Icke 1984; Ganeshaiah Veena et al. 2019). The voids are believed to be most vulnerable to the large-scale tidal effects due to their lowest-densities even at the primordial stages (Park & Lee 2007) and to retain well the imprints of early universe physics due to their pristine nature (Hoyle et al. 2005; Park & Lee 2009; Domínguez-Gómez et al. 2023). Much effort has been made to find optimal void statistics that have the power to put tight constraints on the initial conditions of the universe (e.g., Sheth & van de Weygaert 2004; Park & Lee 2007; Lee & Park 2009; Biswas et al. 2010; Bos et al. 2012; Ricciardelli et al. 2013; Massara et al. 2015; Verza et al. 2019; Hamaus et al. 2020; Rezaei 2020; Davies et al. 2021; Fernández-García et al. 2025).

Very recently, the void spin distribution has been proposed by Kang & Lee (2025) as a probe of the amplitude of initial density power spectrum,  $\sigma_8$ . Despite that the voids expand faster than the rest of the universe, their constituents develop tangential velocities as well as anisotropic spatial distributions within the voids due to the large-scale tidal effects (Shandarin et al. 2006). It was Lee & Park (2006) who first introduced the concept of void spins to effectively describe the deviation of void galaxies from isotropic spatial distributions and radial motions. Defining the angular momentum vectors of voids in the same manner as those of DM halos, Lee & Park (2006) showed that the directions of void angular momenta were strongly aligned with the principal axes of the largest-scale tidal fields, revealing strong connections between the voids and the linear tidal fields.

Using the same definition of the halo spin parameters as in Bullock et al. (2001) for the void spins, Kang & Lee (2025) newly found with the help of  $N$ -body experiments that the void spin distribution is very well approximated by the generalized Gamma model, regardless

of the key cosmological parameters. The Gamma model for the void spin distribution is characterized by two adjustable parameters whose best-fit values turned out to be dependent strongly on  $\sigma_8$  and weakly on  $\Omega_m$ , but insensitive to the other initial conditions considered such as the expansion rate, total neutrino mass ( $M_\nu$ ) and dark energy (DE) equation of state ( $w$ ).

In practice, however, it is not plausible to determine the void spin distribution in real space with high accuracy since it requires information on the 3D peculiar velocities of the void galaxies. To overcome this practical difficulty, Kang & Lee (2025) proposed a scheme based on the novel methodology devised by Wang et al. (2021) to determine the filament spins in 2D redshift-space. According to this scheme, the projected spin axis of a void, if not being parallel to the line of sight direction, would divide the projected void region into two sectors between which significant asymmetry in the void galaxy redshifts is expected to exist. The projected spin axis of a void can be determined as the bisector that yields the maximum redshift asymmetry between the two sectors. The void spins, or equivalently the magnitudes of rotational motions of the void galaxies around the spin axes, should be proportional to this maximum redshift asymmetry.

In the work of Kang & Lee (2025) was considered only two classes of the background cosmologies where the most dominant form of matter contents is the cold dark matter (CDM), while the present acceleration of spacetime is driven either by the cosmological constant ( $\Lambda$ ) with  $w = -1$  or the quintessence scalar field with  $w \neq -1$ . Both classes of the cosmologies assumed the vanilla slow-roll single field inflation potential which produces a power-law spectrum of primordial density fluctuation with scale independent spectral index,  $n_s$ . However, recent measurements of the Lyman- $\alpha$  forest flux spectrum detected a significant signal of  $\alpha_s \equiv dn_s/d \ln k \neq 0$  on the scale of  $k \sim 1 h \text{ Mpc}^{-1}$  (Rogers & Poulin 2025), which could challenge this simple assumption based on the vanilla inflation scenario.

To confirm, however, that the detected signal of  $\alpha_s \neq 0$  is truly caused by the primordial condition rather than by the late-time effects like the presence of warm DM particles (Rogers & Poulin 2025), it is imminently important to determine  $\alpha_s$  with an independent diagnostics on different scales where no late-time effects can produce spurious signals. In light of the finding of Kang & Lee (2025) that the void spin distribution is particularly sensitive to  $\sigma_8$  but independent of the other cosmological parameters including  $M_\nu$ , we speculate that the observable version of void spin distribution, i.e., the redshift asymmetry distribution of voids, could be such a complimentary diagnostics of  $\alpha_s$ .

In this Letter, we are going to first construct a non-parametric model for the redshift asymmetry of voids as a function of initial conditions by analyzing a mock redshift-space dataset obtained from a series of high-resolution  $N$ -body simulations performed for a com-

prehensive broad range of background cosmologies including those with non-zero running of spectral index. Using this non-parametric model, we will investigate how the scale dependence of  $n_s$  affects the redshift asymmetry distribution of voids and explore the efficiency of the void redshift asymmetry distribution as a probe of  $\alpha_s$  on the scales that the previous approaches based on the measurements of primordial power spectrum were unable to cover (e.g., Louis et al. 2025; Calabrese et al. 2025; Rogers & Poulin 2025).

## 2. Physical Analysis

Our numerical analysis relies on the data from the AbacusSummit series of simulations (Maksimova et al. 2021) that were run by applying the ABACUS cosmological  $N$ -body code (Garrison et al. 2021) to  $\sim 330$  billion DM particles with mass resolution of  $2 \times 10^9 h^{-1} M_\odot$  on a periodic box of volume  $8 h^{-3} \text{Gpc}^3$ . The AbacusSummit simulations kept tracks of the DM particles from the initial redshift  $z = 99$  down to  $z = 0.1$  for the most extensive scope of background cosmologies, the initial conditions of which were all efficiently set up according to the Cosmic Linear Anisotropy Solving System (CLASS) (Lesgourgues 2011). From the particle snapshots at redshifts in the range of  $0.1 \leq z \leq 8$  were resolved the bound DM halos via the COMPASO halo-finder that Hadzhiyska et al. (2022) developed by refining the classical spherical over-density algorithm (Warren et al. 1992).

Among the cosmologies covered by the AbacusSummit series are selected three different classes of the background cosmologies for the purpose of the current work. To the first class belongs the flat  $\Lambda$ CDM cosmologies with various values of  $\Omega_m$  and  $\sigma_8$ , including the one with Planck initial conditions (Planck Collaboration et al. 2020). The second class comprises the quintessence DE cosmologies,  $w$ CDM, characterized by time varying equation of states,  $w(a) = w_0 + (1 - a)w_a$  with scale factor  $a$ , what is called, the Chevallier-Polarski-Linder parameterization (Chevallier & Polarski 2001; Linder 2003). These two classes assume that the scalar spectral index,  $n_s$ , is scale independent and thus its running,  $\alpha_s \equiv dn_s/d\ln k$  is zero. In the third class are included the extensions of the standard cosmologies to the scale-dependent spectral index with  $\alpha_s \neq 0$ , which we will call *the running model* throughout this Letter. Figure 1 shows how the selected cosmologies of each class are distributed in the configuration space spanned by  $\Omega_m$ - $\sigma_8$  (left panel), by  $w_0$ - $w_a$  (middle panel) and by  $n_s$ - $\alpha_s$  (right panel). In each panel, the intersection of the vertical and horizontal dashed lines correspond to the configuration of the vanilla  $\Lambda$ CDM cosmology with the Planck initial conditions (Planck Collaboration et al. 2020).

For each cosmology, we select only those DM halos with total masses  $M/(h^{-1} M_\odot) \geq 10^{11.5}$  at  $z = 0.1$ , the lowest redshift available from the AbucusSummit simulations, to create

a sample of galactic halos at the present epoch. Hereafter, we will interchangeably use two terms, galactic halos and galaxies, to refer to the selected DM halos. The mass cutoff value of  $10^{11.5} h^{-1} M_{\odot}$  is chosen to be in line with the minimum mass of the halos whose  $g$ -band flux meets the limit of the Large Synoptic Survey Telescope (LSST) (LSST DESC et al. 2021). To be consistent with real observations where the void spins are found in 2D projected redshift space rather than in 3D real space, we create a mock redshift-space galaxy sample. Under the assumption that the line-of-sight direction to each galactic halo is parallel to the  $\hat{x}_3$ -axis, the line-of-sight component of the redshift-space position of a galaxy located at the real position  $(x_1, x_2, x_3)$  is determined as  $x_{r3} \equiv x_3 + \mathbf{v} \cdot \hat{x}_3 / H_0$  where  $\mathbf{v}$  is the peculiar velocity,  $H_0 \equiv 100 h \text{ km s}^{-1} \text{ Mpc}^{-1}$  (Hamilton 1998). The other two components of the redshift-space position is the same as the real-space counterpart.

Applying the Void-Finder (Hoyle & Vogeley 2002) to this mock redshift-space sample, we identify a void as a union of a maximal sphere and the non-maximal spheres intersecting the maximal one, which fit the volume of an empty region containing no wall galactic halos. The volume of each void is computed with the help of the Monte-Carlo method and then its effective radius,  $R_v$ , is determined as  $R_v \equiv [3V_v/(4\pi)]^{1/3}$  (Lee & Park 2006; Park & Lee 2007). For the detailed description of the classification of the wall and field galactic halos as well as the application of the Void-Finder algorithm to the halo catalogs from the AbacusSummit simulations, we refer the readers to our prior works (Lee & Park 2006; Kang & Lee 2025).

Among the identified voids, we select only those voids within which 15 or more field galaxies above the mass-cut are embedded. If a void is truly spinning, the projection of its spin axis onto the plane of sky will bisect the void into two sectors between which a significant difference exists in the relative peculiar velocities along the line-of-sight direction. One of the two sectors possesses the galaxies whose residual velocities in the direction of  $\hat{x}_3$  relative to the center will be in the direction of  $\hat{x}_3$ , while the galaxies in the other sector will appear to move in the direction of  $-\hat{x}_3$ . Hereafter, a net difference between the rescaled line-of-sight velocities of the galactic halos belonging to the two opposite sectors, will be called the redshift asymmetry,  $\Delta z \equiv \Delta v/c$ .

In real observations, the orientations of the projected spin axes of voids are unlikely to be directly attainable, since it requires information on the 3D counterparts, the measurements of which are greatly hindered by the practical difficulty in determining the peculiar velocities of the void galaxies. Notwithstanding, the orientation of the projected spin axes of voids may be effectively found by employing the same methodology used to find the 2D orientations of filament spin axes (Wang et al. 2021). We randomly generate an orientation angle of a bisector from the  $x_1$  axis in the  $x_1$ - $x_2$  plane, passing through the center of a void. Then,

we calculate the redshift asymmetry between the opposite sides of the bisector. Iterate this process until the randomly generated orientation angle spans a full range from 0 to 180° and see at what orientation angle the redshift asymmetry reaches the maximum value,  $\Delta z_{\max}$ .

In the following, we provide a detailed explanation for how to determine the redshift asymmetry of a void, by employing the same scheme that Wang et al. (2021) devised to determine the filament spins. Let  $\mathbf{x}_{\beta}^{2d}$  denote the comoving position vector of the  $\beta$ -th galaxy belonging to a void consisting of  $N$  members, located at the center  $\mathbf{x}_c^{2d}$  in 2D redshift space normal to the line of sight direction, and let  $\mathbf{v}_{\beta}^{1d}$  be its peculiar velocity along the line of sight. Let also  $\hat{\mathbf{d}}^{2d}$  denote the 2D unit vector parallel to a bisector passing through  $\mathbf{x}_c^{2d}$ . The redshift asymmetry in opposite sectors dichotomized by  $\hat{\mathbf{d}}^{2d}$  is computed as

$$\Delta z = \frac{1}{c} \left| \sum_{\beta=1}^N \sigma_{\beta} \mathbf{v}_{\beta}^{1d} \right|, \quad (1)$$

where  $\sigma_{\beta} \equiv \text{sgn} \left[ \hat{\mathbf{d}} \times (\mathbf{x}_{\beta}^{2d} - \mathbf{x}_c^{2d}) \right]$ . Note that if  $\sigma_{\beta} > 0$  ( $\sigma_{\beta} < 0$ ), then the  $\beta$ -th void galaxy belongs to the counterclockwise (clockwise) sector in the face-on image of its hosting void. We determine the orientation of a bisector,  $\hat{\mathbf{d}}$ , that maximizes  $\Delta z$ , treating it as the projected spin axis of a given void.

Figure 2 illustrates a projected giant void in the  $x_1$ - $x_2$  plane, and shows how the redshift asymmetry of the void galaxies changes as the orientation of the bisector (dashed green line) changes. The bisector that yields the maximum redshift asymmetry,  $\Delta z_{\max}$ , (bottom-left panel) corresponds to the projected 2D spin axis of this void, and this value of  $\Delta z_{\max}$  reflects how rapidly and coherently the void galaxies rotate around the void spin axis. By determining  $\Delta z_{\max}$  of all voids for each cosmology, we numerically determine the probability density distribution,  $p(\Delta z_{\max})$  by dividing the range of the redshift asymmetry into infinitesimally small bins of equal length. The associated uncertainties in the determination of  $p(\Delta z_{\max})$  are computed as Poisson errors at each bin.

Before comparing the redshift asymmetry distributions of voids among the different background cosmologies, however, it is necessary to create  $R_v$ -controlled samples of voids, since the void spins were found to sensitively vary with  $R_v$  (Kang & Lee 2025). Dividing the ranges of  $R_v$  into short intervals, we draw equal number of voids whose effective radii fall in each interval for all of the cosmologies considered to create the  $R_v$ -controlled void samples. Figure 3 plots the number counts of voids as a function of  $R_v$  from the original and controlled samples of voids (left and right panels, respectively). As can be seen, although the original samples of voids greatly differ in their size distributions among the background cosmologies, the controlled samples yield the identical size distributions of voids not only among the cosmologies belonging to the same class but among all of the cosmologies considered.

Recalling the result of Kang & Lee (2025) that the probability density distribution of void spins determined in the 3D real space was well described by the generalized Gamma model regardless of the background cosmology, we also compare the numerically obtained  $p(\Delta z_{\max})$  from the controlled samples with the same distribution:

$$p(\Delta z_{\max}) = \frac{(\Delta z_{\max})^{k-1}}{2\Gamma(2k)\theta^k} \exp\left[-\left(\frac{\Delta z_{\max}}{\theta}\right)^{1/2}\right], \quad (2)$$

where  $\Gamma$  denotes the Gamma function, while  $k$  and  $\theta$  are two characteristic parameters, quantifying the shape and scale of the Gamma distribution, respectively.

The best-fit values of  $k$  and  $\theta$  are determined by fitting Equation (2) to the numerically obtained  $p(\Delta z_{\max})$  via the  $\chi^2$ -minimization process. Figure 4 shows how the best-fit values of  $k$  and  $\theta$  vary with  $\Omega_m$  and  $\sigma_8$  of the background cosmologies considered. The error involved in the determination of each parameter corresponds to the marginalized one standard deviation computed by using the Gaussian model of  $p[-\chi^2(k, \theta)/2]$ . The horizontal shaded dark, light and lightest gray regions correspond to the  $1\sigma$ ,  $2\sigma$  and  $3\sigma$  confidence regions around the best-fit parameters of  $k$  and  $\theta$  for the case of the Planck  $\Lambda$ CDM cosmology (Planck Collaboration et al. 2020). As can be seen, the scale parameter  $\theta$  exhibit sensitive variation with  $\Omega_m$  and  $\sigma_8$ , while the shape parameter  $k$  seem to be almost independent with them. Upon this finding, we set  $k$  at the fixed best-fit value determined for the Planck  $\Lambda$ CDM case, and treat Equation (2) as a single-parameter formula and refit it to the numerical result of  $p(\Delta z_{\max})$  to redetermine the best-fit value of the single parameter,  $\theta$ , for each cosmology via the  $\chi^2$ -minimization.

Figure 5 shows  $p(\Delta z_{\max})$  for nine different cosmologies (black filled circles) and compares them with the analytical Gamma distribution (red solid lines) given in Equation (2) with best-fit value of  $\theta$ . It is worth emphasizing here that the value of  $k$  is fixed at the for all of the nine cosmologies. Despite that we adjust only  $\theta$  of the Gamma distribution, the analytical and numerical results notably agree with each other very well. Although the results only for the nine exemplary cosmologies (three belonging to each of the three classes) are shown in Figure 5, it is confirmed that the single parameter formula validly describes  $p(\Delta z_{\max})$  for all of the 44 cosmologies considered. Recalling the result of Kang & Lee (2025) that the probability density distribution of void spins determined in the 3D real space was well described by the same generalized Gamma distribution, we interpret these good agreements between  $p(\Delta z_{\max})$  and Equation 2 for all of the cosmologies considered as an evidence that the redshift asymmetry distribution of voids measured in projected 2D redshift space indeed reflects well the true void spin distribution in 3D real space.

Noting that for the  $\Lambda$ CDM case, the best-fit value of  $\theta$  of  $p(\Delta z_{\max})$  changes almost linearly with  $\Omega_m$  when  $\sigma_8$  is fixed, and vice versa, we put forth the following bilinear formula

as a non-parametric model for  $\theta$ :

$$\theta_{\text{model}}(\Omega_m, \sigma_8) = \eta_1 \Omega_m + \eta_2 \sigma_8 + \eta_3, \quad (3)$$

where  $\{\eta_i\}_{i=1}^3$  are three coefficients whose values are found via the generalized  $\chi^2$ -statistics to be  $\eta_1 = (9.251 \pm 0.023)10^{-5}$ ,  $\eta_2 = (2.735 \pm 0.015)10^{-5}$ , and  $\eta_3 = (-1.735 \pm 0.016)10^{-5}$  for the  $\Lambda$ CDM case. The left-panel of Figure 6 plots  $\theta_{\text{model}}$  with these best-fit coefficients versus the original scale parameter  $\theta$  for the  $\Lambda$ CDM cosmologies (black filled squares). The shaded dark, light, and lightest gray regions around the straight line of  $\theta = \theta_{\text{model}}$  correspond to the  $1\sigma$ ,  $2\sigma$  and  $3\sigma$  scatters around the best-fits. As can be seen, Equation (3) matches very well the original values of  $\theta$ , for the case of the  $\Lambda$ CDM cosmologies.

For the  $w$ CDM cosmologies, we evaluate  $\theta_{\text{model}}$  by putting their values of  $\Omega_m$  and  $\sigma_8$  into Equation (3), while setting the values of  $\{\eta_i\}_{i=1}^3$  at the same best-fit values for the  $\Lambda$ CDM case, the results of which are shown as green and yellow upside-down triangles in the left panel of Figure 6. As can be seen, the points,  $(\theta, \theta_{\text{model}})$ , are all within  $3\sigma$  from the line of  $\theta = \theta_{\text{model}}$ , even for the  $w$ CDM cases, regardless of the sign of  $w_a$ . Note that Eq. 3 works well for the  $w$ CDM case despite that its coefficients,  $\{\eta_i\}_{i=1}^3$  are fixed at the values obtained for the  $\Lambda$ CDM case. This result indicates an almost universality of Equation (3).

The values of  $\theta_{\text{model}}$  for the running cosmologies are also computed in the same manner, and shown as filled circles whose colors vary from red to blue as  $\alpha_s$  gradually changes from  $-0.04$  to  $0.04$ . As can be seen, the points,  $(\theta, \theta_{\text{model}})$ , depart significantly from the straight line of  $\theta = \theta_{\text{model}}$ . The larger the absolute value of  $\alpha_s$  is, the higher the departure from the straight line is. In our words, Eq. (3) with fixed coefficients no longer holds true for the running cosmologies. A consistent trend is witnessed that if  $\alpha_s > 0$  ( $\alpha_s < 0$ ), then the value of  $\theta_{\text{model}}$  is lower (higher) than  $\theta$ . Since the redshift asymmetry of voids is directly proportional to  $\theta$ , this result indicates that the higher positive (negative) running lead the voids to rotate less (more) rapidly than the case of scale-independent spectral index.

To examine whether or not the redshift asymmetry distribution of voids determined in real-space would yield a similar result, we repeat the whole process but in real space, the results of which are shown in the right-panel of Figure 6. The best-fit coefficients of  $\theta_{\text{model}}$  in real-space are found to be  $\eta_1 = (8.258 \pm 0.022)10^{-5}$ ,  $\eta_2 = (2.434 \pm 0.014)10^{-5}$ , and  $\eta_3 = (-1.61 \pm 0.016)10^{-5}$  for the  $\Lambda$ CDM class. Although the coefficient values differ between the real and redshift space cases, the same phenomenon is found:  $\theta_{\text{model}}$  given in Equation (3) is universally valid in describing the scale parameter of the redshift asymmetry distribution of voids, only provided that the running of scalar spectral index is zero. The break-down of the universality of Equation (3) for the running model implies that the redshift asymmetry distribution of voids can put a stringent test to the vanilla single-field slow-roll inflation model in which  $\alpha_s = 0$ . Furthermore, those inflation models that predict different values

of  $\alpha_s$  can also be constrained by comparing  $\theta_{\text{model}}$  and the value of  $\theta$  from the observable redshift asymmetry distribution of voids.

### 3. Discussion and Conclusion

The latest observations of the Lyman- $\alpha$  forest flux power spectrum from the extended Baryon Oscillation Spectroscopic Survey (eBOSS) (Chabanier et al. 2019) detected a significant signal of  $\alpha_s < 0$  on the scale of  $k \gtrsim 1 h \text{ Mpc}^{-1}$  (Rogers & Poulin 2025). It poses not only a challenge to the vanilla single-field slow-roll inflation paradigm which assumes  $\alpha_s = 0$  but also an inconsistency with the recent measurements of the cosmic microwave background (CMB) radiation from the Atacama Cosmology Telescope Data Release 6 (ACT DR6) that hinted  $\alpha_s > 0$  (Louis et al. 2025; Calabrese et al. 2025). Given the scale difference between those two probes, their inconsistency on the value of  $\alpha_s$  implied that the primordial density power spectrum might have a compound shape deviating from a simple power-law with scale independent spectral index envisioned in the standard vanilla model of inflation.

It was, however, pointed out by Rogers & Poulin (2025) that their result, the negative value of  $\alpha_s$ , found from the eBOSS observation might be caused by the late-time effects, e.g., the small-scale suppression due to the presence of ultra-light axion or warm DM particles. Moreover, the positive value of  $\alpha_s > 0$  found in the CMB data from the ACT DR6 was not interpreted as a strong counter evidence against the scale independence of  $n_s$  due to relatively large errors associated in the determination of  $\alpha_s$  on the large-scale. This inconsistency and difficulty in identifying the true cause of non-zero value of  $\alpha_s$  stems from the simple fact that the standard diagnostics, the matter density power spectrum, inherently suffers from strong degeneracy among many different factors including the key cosmological parameters as well as the nature of DM and DE.

To overcome this degeneracy, what is required is a new independent diagnostics by which  $\alpha_s$  can be directly determined without measuring the matter density power spectrum. Here, we have demonstrated that the redshift asymmetry distribution of voids can be such a complimentary probe of  $\alpha_s$ . The coherent rotations of the galaxies inside spinning voids can be observed as maximum redshift asymmetry around the bisectors parallel to the projected spin axes of hosting voids. To numerically determine the redshift asymmetry distribution of voids and to investigate its dependence on the initial conditions, we have analyzed ample datasets from the AbacusSummit series of simulations for the 44 different background cosmologies that include the standard vanilla model with  $w = -1$  and  $\alpha_s = 0$  ( $\Lambda$ CDM) and two extensions of the vanilla  $\Lambda$ CDM model to the cases of  $w \neq -1$  ( $w$ CDM) and  $\alpha_s \neq 0$  (running). We have chosen those background cosmologies belonging to these three classes

that have all different values of  $\Omega_m$  and  $\sigma_8$ , the two key cosmological parameters only to which the void spin distribution were found to be sensitive (Kang & Lee 2025).

Just like the void spin distribution, the redshift asymmetry distribution of voids from the mock redshift-space sample in the projected 2D space has turned out to be excellently described by the generalized Gamma model characterized by the shape and the scale parameters. It has been found that the shape parameter,  $k$ , of this distribution behaves like a constant independent of the background cosmology, while the scale parameter,  $\theta$ , exhibits a bilinear scaling with  $\Omega_m$  and  $\sigma_8$ . Constructing a non-parametric linear model for  $\theta$  as a function of  $\Omega_m$  and  $\sigma_8$ , we have demonstrated that this model,  $\theta_{\text{model}}$ , is valid for all of the  $\Lambda$ CDM and  $w$ CDM cosmologies considered, even though its three coefficients are fixed at the best-fit values obtained for the case of the  $\Lambda$ CDM cosmologies. Discovering that the scale parameter of the redshift asymmetry distribution of voids depart from the universal value,  $\theta_{\text{model}}$ , only for the case of the running model, we have witnessed a clear and consistent trend that a more positive (negative) value of the running yields a lower (higher) degree of redshift asymmetry of voids. A critical implication of this result is that the comparison of the redshift asymmetry distribution of voids with the universal model is capable of constraining the values of  $\alpha_s$  on the void scales, a few tens of Mpc.

It is worth mentioning here a couple of advantages of using the redshift asymmetry distribution of voids as a new diagnostics of  $\alpha_s$ . First of all, it requires information only on the redshifts of void galaxies in the local universe, the measurements of which have achieved the unprecedently high 1% accuracy level in the currently available data from the latest galaxy surveys (Alam et al. 2015). Second, it is based on the angular momentum fields that can shed a new light on the primordial state of the universe, which cannot be probed by those standard diagnostics based on the matter density and peculiar velocity fields (Motloch et al. 2021). Third, it probes the scale-dependence of  $n_s$  on the intermediate scales,  $k/(h \text{ Mpc}^{-1}) \sim 0.1$ , which were not spanned by the previous CMB and Lyman- $\alpha$  forest observations. Our future work will be in the direction of testing the vanilla inflation models by applying this new diagnostics to real voids from the latest observations.

G.K. acknowledges that this research was supported by Basic Science Research Program through the National Research Foundation of Korea (NRF) funded by the Ministry of Education (RS-2025-25408975). J.L. acknowledges the support by Basic Science Research Program through the NRF of Korea funded by the Ministry of Education (RS-2025-00512997).

## REFERENCES

Alam, S., Albareti, F. D., Allende Prieto, C., et al. 2015, *ApJS*, 219, 1, 12. doi:10.1088/0067-0049/219/1/12

Biswas, R., Alizadeh, E., & Wandelt, B. D. 2010, *Phys. Rev. D*, 82, 2, 023002. doi:10.1103/PhysRevD.82.023002

Bond, J. R., Kofman, L., & Pogosyan, D. 1996, *Nature*, 380, 6575, 603. doi:10.1038/380603a0

Bos, E. G. P., van de Weygaert, R., Dolag, K., et al. 2012, *MNRAS*, 426, 1, 440. doi:10.1111/j.1365-2966.2012.21478.x

Bullock, J. S., Dekel, A., Kolatt, T. S., et al. 2001, *ApJ*, 555, 1, 240. doi:10.1086/321477

Calabrese, E., Hill, J. C., Jense, H. T., et al. 2025, *JCAP*, 2025, 11, 063. doi:10.1088/1475-7516/2025/11/063

Cautun, M., van de Weygaert, R., Jones, B. J. T., et al. 2014, *MNRAS*, 441, 4, 2923. doi:10.1093/mnras/stu768

Chabanier, S., Palanque-Delabrouille, N., Yèche, C., et al. 2019, *JCAP*, 2019, 7, 017. doi:10.1088/1475-7516/2019/07/017

Chevallier, M. & Polarski, D. 2001, *International Journal of Modern Physics D*, 10, 2, 213. doi:10.1142/S0218271801000822

Davies, C. T., Cautun, M., Giblin, B., et al. 2021, *MNRAS*, 507, 2, 2267. doi:10.1093/mnras/stab2251

Domínguez-Gómez, J., Pérez, I., Ruiz-Lara, T., et al. 2023, *Nature*, 619, 7969, 269. doi:10.1038/s41586-023-06109-1

Einasto, J. 2006, *Communications of the Konkoly Observatory Hungary*, 104, 163. doi:10.48550/arXiv.astro-ph/0609686

Feldbrugge, J. & van de Weygaert, R. 2023, *JCAP*, 2023, 2, 058. doi:10.1088/1475-7516/2023/02/058

Feldbrugge, J., Yan, Y., & van de Weygaert, R. 2023, *MNRAS*, 526, 4, 5031. doi:10.1093/mnras/stad2777

Feldbrugge, J. & van de Weygaert, R. 2025, *MNRAS*, 539, 2, 873. doi:10.1093/mnras/staf536

Fernández-García, E., Betancort-Rijo, J. E., Prada, F., et al. 2025, *A&A*, 695, A19. doi:10.1051/0004-6361/202451264

Galárraga-Espinosa, D., Cadiou, C., Gouin, C., et al. 2024, *A&A*, 684, A63. doi:10.1051/0004-6361/202347982

Ganeshaiah Veena, P., Cautun, M., Tempel, E., et al. 2019, *MNRAS*, 487, 2, 1607. doi:10.1093/mnras/stz1343

Garrison, L. H., Eisenstein, D. J., Ferrer, D., et al. 2021, *MNRAS*, 508, 1, 575. doi:10.1093/mnras/stab2482

Hadzhiyska, B., Eisenstein, D., Bose, S., et al. 2022, *MNRAS*, 509, 1, 501. doi:10.1093/mnras/stab2980

Hahn, O., Porciani, C., Carollo, C. M., et al. 2007, *MNRAS*, 375, 2, 489. doi:10.1111/j.1365-2966.2006.11318.x

Hamaus, N., Pisani, A., Choi, J.-A., et al. 2020, *JCAP*, 2020, 12, 023. doi:10.1088/1475-7516/2020/12/023

Hamilton, A. J. S. 1998, *The Evolving Universe*, 231, 185. doi:10.1007/978-94-011-4960-0\_17

Hoyle, F. & Vogeley, M. S. 2002, *ApJ*, 566, 2, 641. doi:10.1086/338340

Hoyle, F., Rojas, R. R., Vogeley, M. S., et al. 2005, *ApJ*, 620, 2, 618. doi:10.1086/427176

Icke, V. 1984, *MNRAS*, 206, 1P. doi:10.1093/mnras/206.1.1P

Kang, G. & Lee, J. 2025, *JCAP*, 2025, 6, 011. doi:10.1088/1475-7516/2025/06/011

Kuhlman, B., Melott, A. L., & Shandarin, S. F. 1996, *ApJ*, 470, L41. doi:10.1086/310298

Lee, J. & Park, D. 2006, *ApJ*, 652, 1, 1. doi:10.1086/507936

Lee, J. & Park, D. 2009, *ApJ*, 696, 1, L10. doi:10.1088/0004-637X/696/1/L10

Lesgourgues, J. 2011, , arXiv:1104.2932. doi:10.48550/arXiv.1104.2932

Linder, E. V. 2003, *Phys. Rev. Lett.*, 90, 9, 091301. doi:10.1103/PhysRevLett.90.091301

Louis, T., La Posta, A., Atkins, Z., et al. 2025, *JCAP*, 2025, 11, 062. doi:10.1088/1475-7516/2025/11/062

Abolfathi, B., Alonso, D., et al. 2021, *ApJS*, 253, 1, 31. doi:10.3847/1538-4365/abd62c

Lu, Y. S., Mandelker, N., Oh, S. P., et al. 2024, MNRAS, 527, 4, 11256. doi:10.1093/mnras/stad3779

Maksimova, N. A., Garrison, L. H., Eisenstein, D. J., et al. 2021, MNRAS, 508, 3, 4017. doi:10.1093/mnras/stab2484

Massara, E., Villaescusa-Navarro, F., Viel, M., et al. 2015, JCAP, 2015, 11, 018. doi:10.1088/1475-7516/2015/11/018

Motloch, P., Yu, H.-R., Pen, U.-L., et al. 2021, Nature Astronomy, 5, 283. doi:10.1038/s41550-020-01262-3

Planck Collaboration, Aghanim, N., Akrami, Y., et al. 2020, A&A, 641, A6. doi:10.1051/0004-6361/201833910

Park, D. & Lee, J. 2007, Phys. Rev. Lett., 98, 8, 081301. doi:10.1103/PhysRevLett.98.081301

Park, D. & Lee, J. 2009, MNRAS, 397, 4, 2163. doi:10.1111/j.1365-2966.2009.15117.x

Pearson, R. C. & Coles, P. 1995, MNRAS, 272, 1, 231. doi:10.1093/mnras/272.1.231

Ramachandra, N. S. & Shandarin, S. F. 2015, MNRAS, 452, 2, 1643. doi:10.1093/mnras/stv1389

Rezaei, Z. 2020, ApJ, 902, 2, 102. doi:10.3847/1538-4357/abb59d

Ricciardelli, E., Quilis, V., & Planelles, S. 2013, MNRAS, 434, 2, 1192. doi:10.1093/mnras/stt1069

Rogers, K. K. & Poulin, V. 2025, Physical Review Research, 7, 1, L012018. doi:10.1103/PhysRevResearch.7.L012018

Shandarin, S. F., Sheth, J. V., & Sahni, V. 2004, MNRAS, 353, 1, 162. doi:10.1111/j.1365-2966.2004.08060.x

Shandarin, S., Feldman, H. A., Heitmann, K., et al. 2006, MNRAS, 367, 4, 1629. doi:10.1111/j.1365-2966.2006.10062.x

Sheth, R. K. & van de Weygaert, R. 2004, MNRAS, 350, 2, 517. doi:10.1111/j.1365-2966.2004.07661.x

Sousbie, T., Pichon, C., Colombi, S., et al. 2008, MNRAS, 383, 4, 1655. doi:10.1111/j.1365-2966.2007.12685.x

Verza, G., Pisani, A., Carbone, C., et al. 2019, JCAP, 2019, 12, 040. doi:10.1088/1475-7516/2019/12/040

Wang, P., Libeskind, N. I., Tempel, E., et al. 2021, Nature Astronomy, 5, 839. doi:10.1038/s41550-021-01380-6

Warren, M. S., Quinn, P. J., Salmon, J. K., et al. 1992, ApJ, 399, 405. doi:10.1086/171937

Wilding, G., Nevenzeel, K., van de Weygaert, R., et al. 2021, MNRAS, 507, 2, 2968. doi:10.1093/mnras/stab2326

Zel'dovich, Y. B. 1970, A&A, 5, 84.

Zeldovich, I. B., Einasto, J., & Shandarin, S. F. 1982, Nature, 300, 5891, 407. doi:10.1038/300407a0

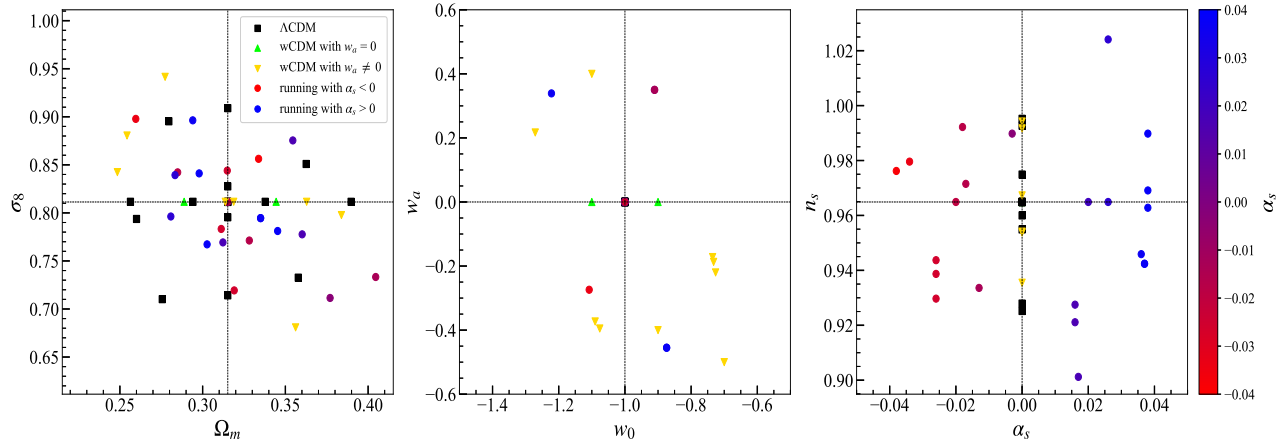


Fig. 1.— Configurations of three classes of 44 different background cosmologies in 2D spaces spanned by  $\Omega_m$ - $\sigma_8$  (left panel), by  $w_0$ - $w_a$  (middle panel) and by  $n_s$ - $\alpha_s$  (right panel).

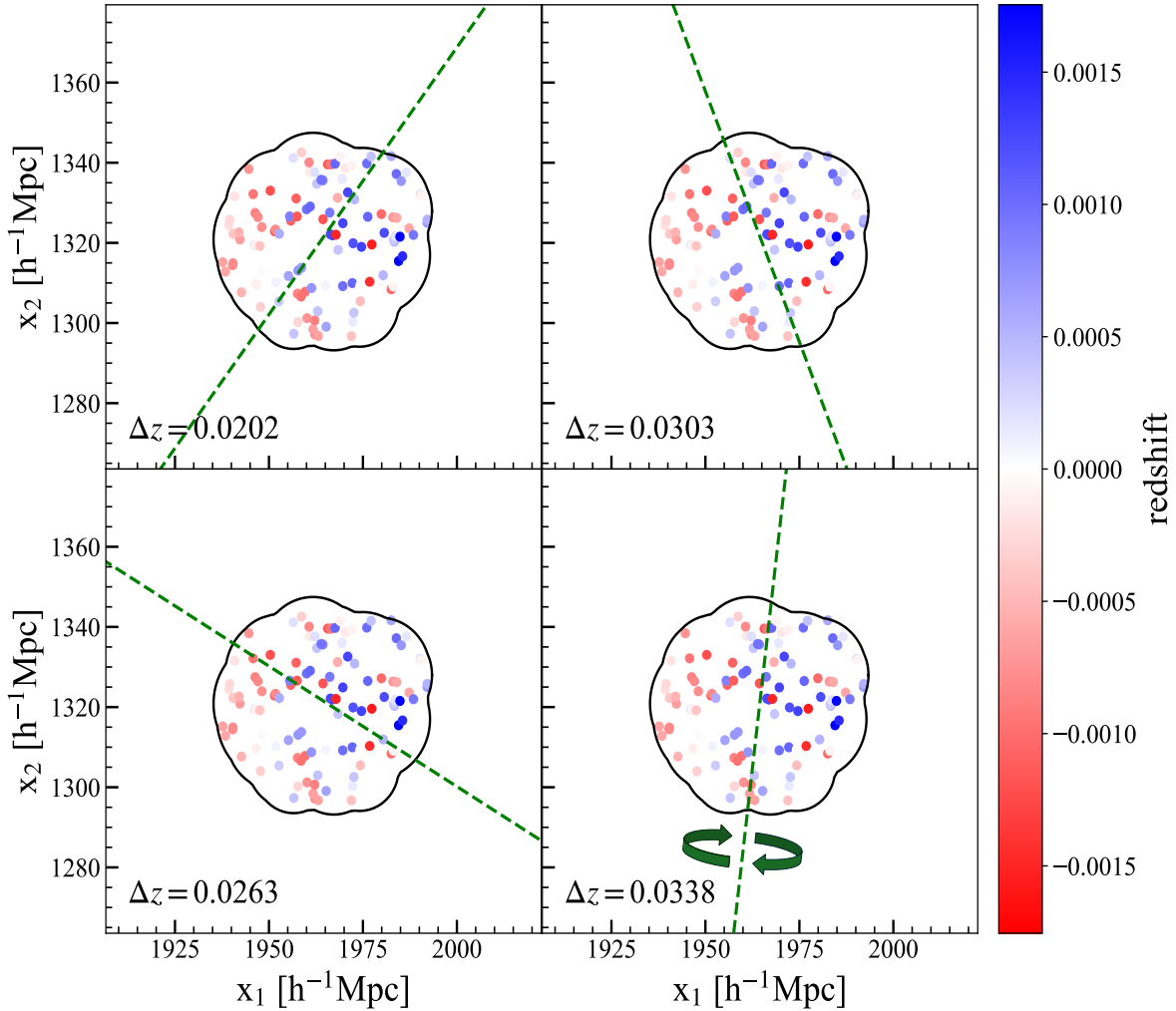


Fig. 2.— Illustration of the dependence of redshift asymmetry of void galaxies on the orientation of the bisector axes.

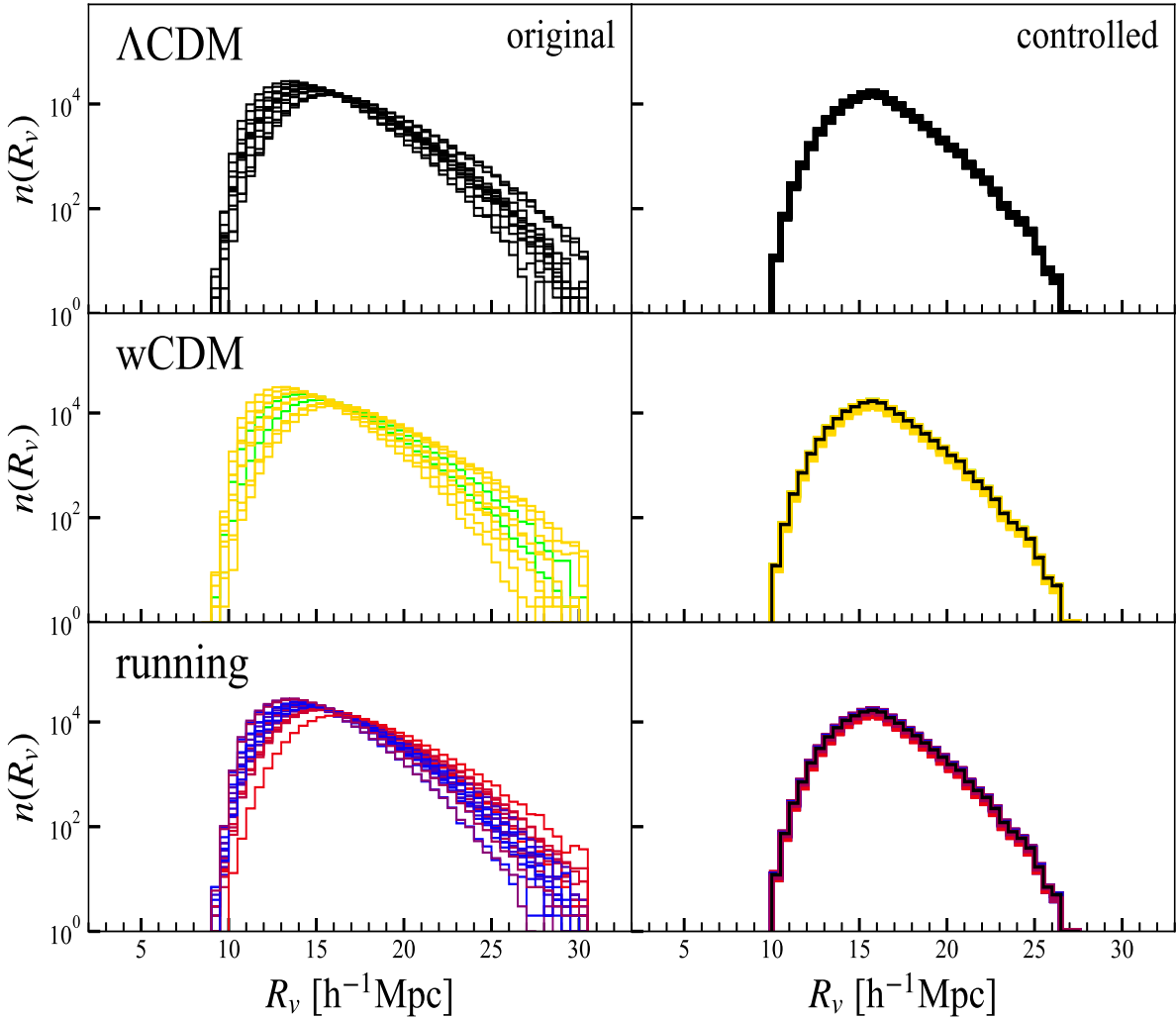


Fig. 3.— Original and controlled distributions of the void sizes for the three classes of the background cosmologies in the left and right panels, respectively. Note that the controlled size distributions of void are identical over the three classes.

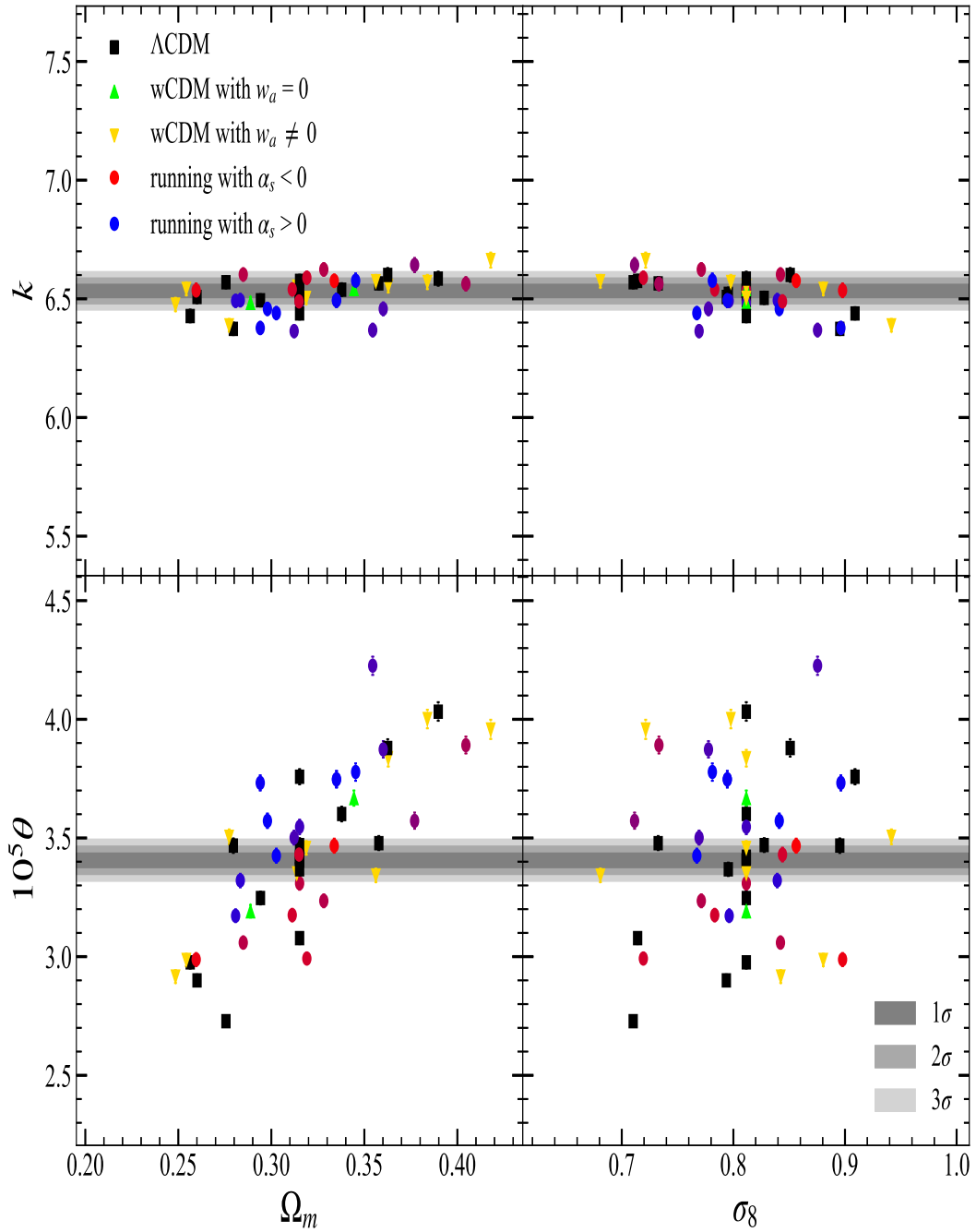


Fig. 4.—  $\Omega_m$  and  $\sigma_8$  variations of two parameters,  $k$  and  $\theta$ , of the generalized  $\Gamma$ -model for the void redshift asymmetry distribution in the left and right panels, respectively.

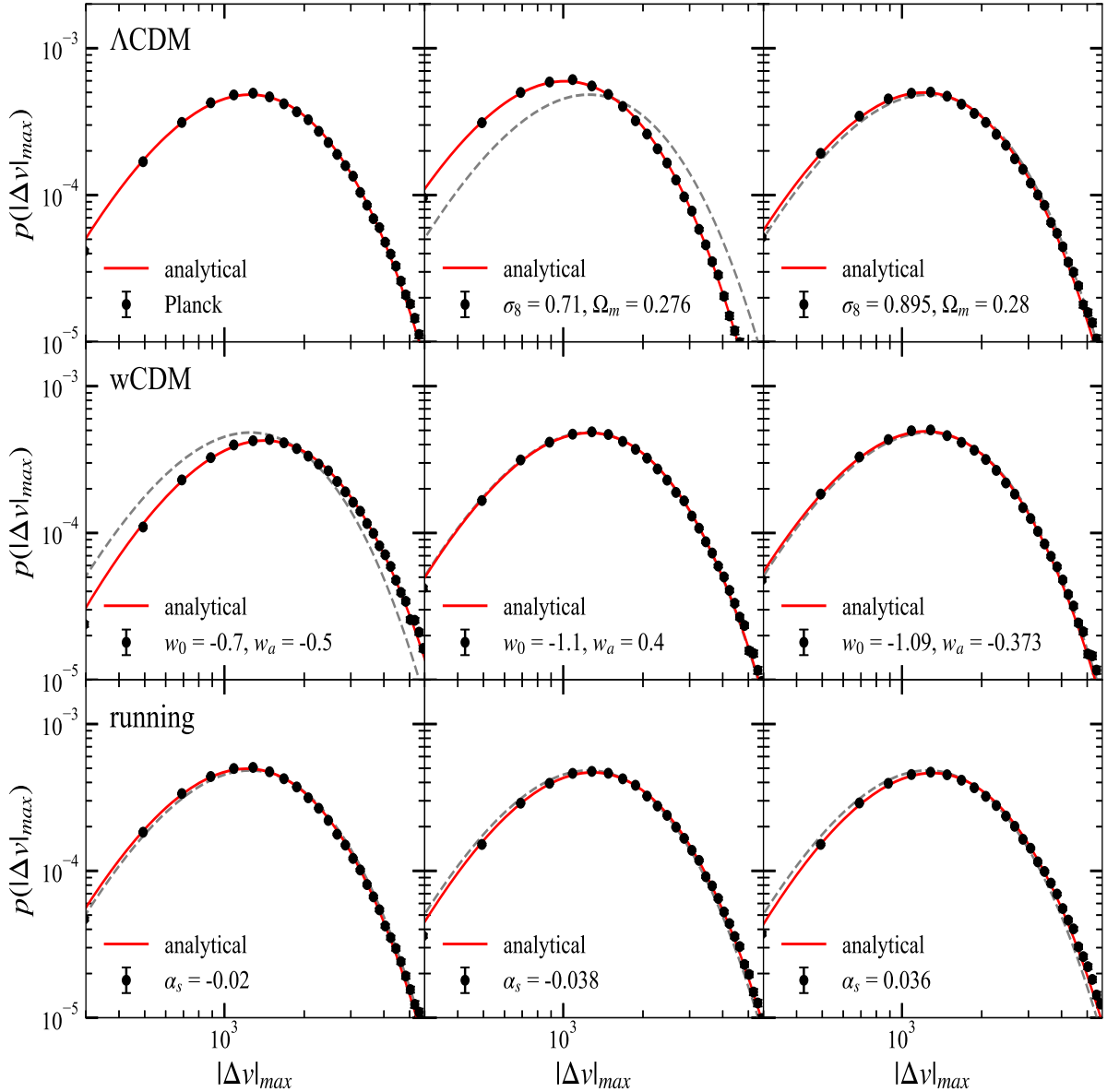


Fig. 5.— Numerically obtained probability density distributions of void redshift asymmetry (filled black circles) compared with the best-fit  $\Gamma$ -models (red solid line) for the three different classes of the cosmologies.

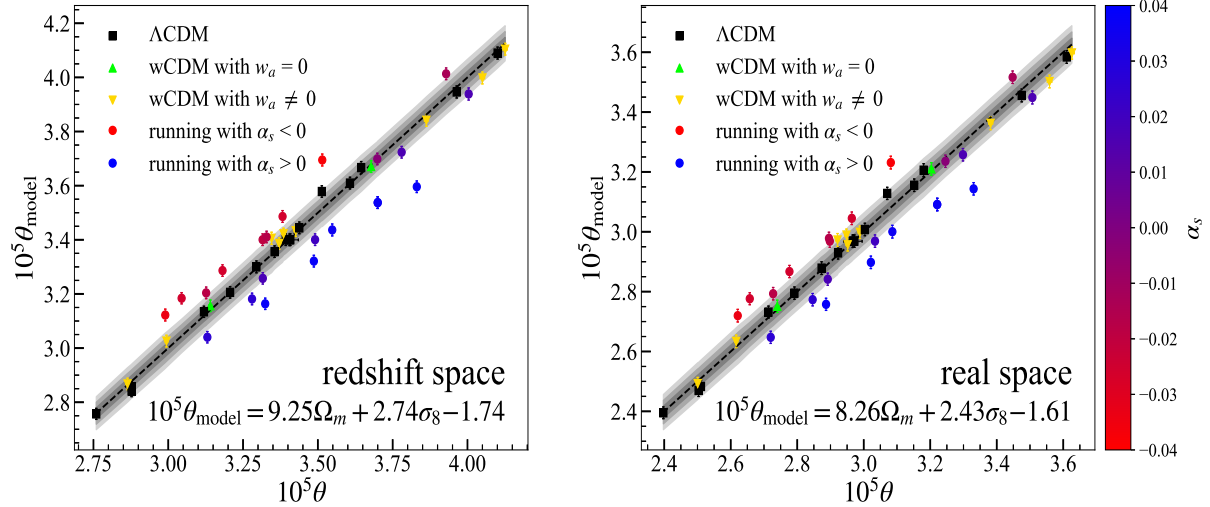


Fig. 6.— Configurations of the three classes of the background cosmologies in the two dimensional space spanned by  $\theta$ - $\theta_{\text{model}}$ . The shaded (dark, light and lightest) gray-color area correspond to the 68%, 95% and 99% confidence regions around the best-fit  $\theta_{\text{model}}$  determined for the  $\Lambda$ CDM cosmology.